Electron Paramagnetic Resonance Spectroscopic Measurement of Mn^{2+} Binding Affinities to the Hammerhead Ribozyme and Correlation with Cleavage Activity†

Thomas E. Horton, D. Roxanne Clardy, and Victoria J. DeRose*

Department of Chemistry, Texas A&M University, College Station, Texas 77842-3012

Received June 16, 1998; Revised Manuscript Received October 16, 1998

ABSTRACT: Efficient phosphodiester bond cleavage activity by the hammerhead ribozyme requires divalent cations. Toward understanding this metal ion requirement, the Mn^{2+}-binding properties of hammerhead model ribozymes have been investigated under dilute solution conditions, using electron paramagnetic resonance spectroscopy (EPR) to detect free Mn^{2+} in the presence of added ribozyme. Numbers and affinities of bound Mn^{2+} were obtained at pH 7.8 (5 mM triethanolamine) in the presence of 0, 0.1, and 1.0 M NaCl for an RNA−DNA model consisting of a 13-nucleotide DNA "substrate" hybridized to a 34-nucleotide RNA "enzyme" [Pley, H. W., Flaherty, K. M., and McKay, D. B. (1994) *Nature 372*, 68−74]. In 0.1 M NaCl, two classes of Mn^{2+} sites are found with $n_1 = 3.7 \pm 0.4$, $K_{d(1)} = 4 \pm 1$ μM (type 1) and $n_2 = 5.2 \pm 0.4$, $K_{d(2)} = 460 \pm 130$ μM (type 2). The high-affinity type 1 sites are confirmed for an active RNA−RNA hybrid (34-nucleotide RNA enzyme:13-nucleotide RNA substrate) by EPR measurements at low Mn^{2+} concentrations. Decreasing NaCl concentration results in an increased number of bound Mn^{2+} per hammerhead. By contrast, a binding titration in 1 M NaCl indicates that a single Mn^{2+} site with apparent $K_d \sim 10$ μM is populated in low concentrations of Mn^{2+}, and apparent cooperative effects at higher Mn^{2+} concentrations result in population of a similar total number of Mn^{2+} sites (n_t = 8−10) as found in 0.1 M NaCl. Mn^{2+}-dependent activity profiles are similar for the active RNA−RNA hybrid in 0.1 and 1 M NaCl. Correlation with binding affinities determined by EPR indicates that hammerhead activity in 0.1 M NaCl is only observed after all four of the high-affinity Mn^{2+} sites are occupied, rises with population of the type 2 sites, and is independent of Mn^{2+} concentrations corresponding to >8−9 Mn^{2+} bound per hammerhead. Equivalent measurements in 1 M NaCl demonstrate a rise in activity with the cooperative transition observed in the Mn^{2+} binding curve. These measurements indicate that, over this NaCl concentration range, hammerhead ribozyme activity is influenced by population of a specific set of divalent cation sites.

RNA molecules that perform chemical reactions, ribozymes, have provoked interest for their roles in biological activities and their potential use as therapeutic agents (*1*, *2*). Most RNA molecules that perform site-specific phosphodiester bond cleavage reactions require divalent cations for maximal activity (*3*, *4*), leading to their classification as metalloenzymes or metalloribozymes (*5*). Potential roles for cations in ribozyme activities include both stabilization of specific RNA conformations and direct interaction with moieties at the catalytic site.

The best-characterized ribozyme to date is the hammerhead motif, depicted in Figure 1 as RNA "enzyme" and "substrate" components (reviewed in refs *6*−*9*). The hammerhead, a highly truncated version of the native self-cleaving tobacco ringspot virus RNA sequence, consists of a conserved core of nucleotides stabilized by three base-paired stems. In the presence of divalent cations, the hammerhead ribozyme specifically cleaves the phosphodiester bond between residues 17 and 1.1 with a mechanism involving nucleophilic attack of the sugar 2′ hydroxide on phosphorus of its neighboring phosphodiester bond, resulting in 2′,3′-cyclic phosphate and 5′-OH as products.

Recent crystallographic models of the hammerhead indicate a Y-shaped structure shown in Figure 1c, in which stems II and III are roughly coaxial and stem I is rotated near to stem II. The initial crystallographic results of Pley et al. (*10*) of an RNA−DNA duplex hammerhead, with sequence identical to that shown in Figure 1a, demonstrate occupancy of a single divalent metal site in crystals soaked in either Mn^{2+} or Cd^{2+}. This site in stem II has contributions from A9 and G10.1 (Figure 1c). By contrast, the subsequent crystallographic results of Scott et al. (*11*, *12*) obtained for an RNA−RNA duplex hammerhead (Figure 1b) show occupancy of at least five sites by either Mn^{2+} or Mg^{2+} ions. Hammerhead crystal structures have now been reported indicating multiple binding sites for Co^{2+} (*13*), Zn^{2+} (*13*), and Tb^{3+} (*14*).

In most hammerhead X-ray crystal structures to date, the cleavage site 2′-OH is not in position to effect the required in-line attack at the phosphodiester bond. Scott et al. have observed intriguing pH-dependent differences in an all-RNA hammerhead (*12*), however, wherein an additional metal ion and a movement in position of the cleavage site phosphodi-

† This work was supported by the NSF (Career), the Robert A. Welch Foundation, and the Texas Higher Education Coordinating Board Advanced Research Program. V.J.D. is a Cottrell Scholar of the Research Corporation.

* Corresponding author: Phone 409-862-1401; FAX 409-845-4719; email derose@mail.chem.tamu.edu.

10.1021/bi981425p CCC: $15.00
Published on Web 12/05/1998

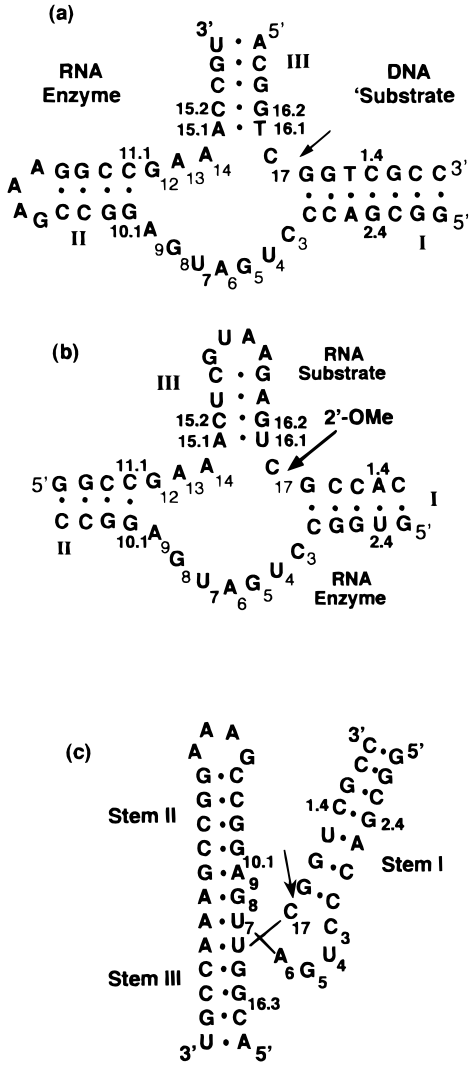

FIGURE 1: Hammerhead ribozyme sequences used in this study and by (a) Pley et al. (*10*) and (b) Scott *et al*. (*11*) for X-ray crystallography. The schematic shown in panel c is based on X-ray crystallographic results of both sequences. Both DNA and RNA substrate strands of hammerhead (a) were used in this study. The substrate strand in panel b has a 2′-*O*-methyl modification at C17.

ester bond are found in crystals poised at pH 8.5 relative to the structure solved at pH 5.5. An additional conformational intermediate was trapped by use of a modified, slow-cleaving hammerhead (*13*). This structure exhibits more extensive changes at the cleavage site that, although the 3.1 Å resolution structure precluded good definition of the scissile bond, require the phosphodiester bond to be very distorted from A-form geometry as is required for the in-line attack mechanism (*13*). Results from solution NMR measurements (*15*) and molecular modeling (*16*) indicate potential structural rearrangements following the cleavage step.

The hammerhead is specifically activated by addition of divalent cations, showing a steep rise in observed rate constant over a relatively narrow range of added metal (*17, 18*). Previous studies report evidence for the importance of potential metal sites both near to the cleavage site and ≥10 Å distant. It has been proposed that ribozymes may use two or more metal ions that play multiple roles in catalysis (*5, 19, 20, 22*). A metal hydroxide is a reasonable candidate to deprotonate and thereby enhance nucleophilicity of the sugar 2′-OH. Involvement of a metal hydroxide in the hammerhead reaction has been suggested on the basis of pH−reactivity profiles of various divalent metal ions (*18*). In addition, metal ion coordination to the cleavage site phosphodiester *pro-*R_p oxygen has been predicted from phosphorothioate-substitution experiments (*17, 21*) although this conclusion has been questioned by Taira and co-workers (*22*). Metal coordination to the cleavage site phosphodiester is thought to be important to delocalize negative charge on the substrate phosphodiester bond.

Other studies point to the importance of metal sites that (according to crystallography) are at positions far from the cleavage site. The effects of phosphorothioate substitutions at the phosphate group responsible for metal ion coordination at A9/G10.1, which is >10 Å from the cleavage site, have recently been interpreted in terms of stabilization of the transition state of the reaction (*23*). In addition, substitution of Tb^{3+} at a site close to G5 apparently inhibits the cleavage reaction (*14*). This result is intriguing because G5 is approximately 10 Å from the cleavage site in current X-ray structures, but mutations of any substituents of G5 reduce cleavage activity (*7*). In addition to these activity measurements, both native gel studies (*24*) and fluorescence resonance energy transfer experiments (*25, 26*) have predicted RNA tertiary structure changes as a function of divalent metal ion concentration.

These studies point to specific contributions of metal ions to structural and chemical aspects of the cleavage reaction. At present, however, there are no direct measurements of the numbers and affinities of divalent metal ions bound to the hammerhead ribozyme in solution. For conventional protein-based metalloenzymes, metal-based spectroscopic techniques such as electron paramagnetic resonance (EPR) have provided structural and mechanistic information, and such studies have potential to increase the tools available to probe metals in catalytic RNA molecules. The paramagnetic ion Mn^{2+} substitutes for the native Mg^{2+} in promoting hammerhead ribozyme activity (*17, 18*) and the EPR signal from Mn^{2+} provides a specific probe of the metal ion environment in the RNA molecule. Metal ion−RNA affinities and the number of metal binding sites can be obtained by taking advantage of the small but measurable effect on the EPR signal as a function of Mn^{2+}−ligand geometry (*27*−*31*). Here we report EPR-based Mn^{2+} binding studies and their relationship with activity measurements in the hammerhead ribozyme.

MATERIALS AND METHODS

RNA Synthesis and Purification. The 34-nucleotide (nt) RNA enzyme with sequence shown in Figure 1a and the 16-nt RNA enzyme strand of Figure 1b were synthesized by in vitro transcription with T7 RNA polymerase (*32*). RNA transcripts were purified by electrophoresis on 20% polyacrylamide gels and electroeluted from the gel slice. Eluted transcripts were dialyzed against the appropriate buffer for at least 48 h with several reservoir changes, concentrated (Centricon-3, Amicon), ethanol-precipitated, and resuspended into the same buffer to form a stock solution. The 13-nt DNA and RNA "substrates" of Figure 1a were purchased (Integrated DNA Technologies), gel-purified, and dialyzed as described for in vitro synthesized RNA. A 25-nt RNA sequence (Figure 1b) with a single 2′-*O*-methyl substituent

at the cleavage site also was purchased (Midland Chemicals) and used following ethanol precipitation and extensive dialysis. All RNA and DNA oligonucleotides used in these studies were ≥90% pure (full-length sequence) as judged by quantitation using high-performance liquid chromatography (HPLC) or matrix-assisted laser desorption ionization (MALDI) mass spectrometry.

Metal-binding titrations and activity studies were carried out in a buffer consisting of 5 mM triethanolamine (TEA) at pH 7.8 and concentrations of 0, 0.1, or 1.0 M NaCl. TEA, a large cation that has little Mn^{2+} and Mg^{2+} association and is not expected to significantly interact with nucleic acids, was chosen for comparison with results from previous Mn^{2+} EPR investigations of tRNA (*30*). In our initial investigations we found a small diminution of the Mn^{2+} EPR signal due to Tris buffer alone, in comparison with a Mn^{2+} EPR standard lacking Tris; no such effect is observed with the TEA buffer. Initial studies were carried out in 100 mM NaCl in order to reduce nonspecific charge-screening effects. Contaminating divalent cations were removed by treatment with Chelex. The "0 M" NaCl RNA samples had an estimated Na^+ concentration of ≤20 μM. All nucleic acids were quantitated by absorbances at 260 nm using calculated extinction coefficients (*33*).

EPR Measurements. To form the RNA−DNA or RNA−RNA hybrid hammerheads, oligonucleotides were combined in a 1:1 ratio in TEA, pH 7.8, heated to 90 °C for 90 s, and cooled on ice for 30 min. EPR titrations were performed at hybrid concentrations of 1−20 μM. Mn^{2+} was added as $MnCl_2$ (American Analytical, ultrapure grade) to the given concentration, using freshly prepared stock solutions. No changes in pH of the buffered samples due to added metal ion were observed. $MnCl_2$ standard samples were prepared in the same TEA/NaCl buffer.

X-band EPR was performed at room temperature with a Bruker ESP-300 spectrometer and TE_{102} cavity. For room-temperature EPR, a sample holder modified from Eaton and Eaton (*34*) consisting of three flat glass slides (Vitrocon, Mountain Lakes, NJ) was filled by capillary action and sealed with Mylar tape. Quartz capillary sample holders were used for higher-concentration Mn^{2+} samples. Reproducibility in EPR signal amplitudes measured on the same day was ±∼2% and sensitivity was approximately 1 μM Mn^{2+}. Mn^{2+} EPR signal intensities were measured under the following conditions: 0.2 mW microwave power, 26 G modulation amplitude, 7.3 G/s scan rate, average of 1−8 scans.

Metal-Binding Titrations Based on Mn^{2+} EPR Signal Amplitudes. The six-line EPR signal from Mn^{2+} ($S = {}^5/_2$, $I = {}^5/_2$) in an octahedral environment arises from the superposition of five sets of degenerate transitions. Binding to a biomolecule can induce a small ligand field asymmetry, causing the transitions to become nondegenerate and resulting in line-broadening whose effect is enhanced by the increase in rotational correlation time for the bound ion. Together these effects strongly attenuate the amplitude of the six-line EPR signal from the bound Mn^{2+}, and under standard detection conditions the bound Mn^{2+} does not contribute to the room-temperature EPR signal. Phenomenologically, this effect can be used to quantitate free Mn^{2+} in aqueous solution [octahedral $Mn(H_2O)_6^{2+}$] versus Mn^{2+} bound to a biological ligand (*27*, *28*). In this technique, the EPR signal intensity of the Mn^{2+}−ligand sample is compared with that of a Mn^{2+} standard, and the difference in signal intensities is assumed to be due to bound Mn^{2+}. Mn^{2+} EPR spectroscopy previously has been used to obtain numbers and affinities of Mn^{2+} binding to proteins (*27*, *28*), tRNA (*30*), and other oligonucleotides (*31*).

Metal-RNA binding isotherms were constructed by plotting the concentration of bound Mn^{2+} divided by the concentration of hybrid in solution ($[Mn_b^{2+}]$/[hyb]) versus the concentration of free Mn^{2+} ($[Mn_f^{2+}]$). Free Mn^{2+} was determined by comparison of signal intensities with a standard curve, which consisted of EPR signal amplitudes versus Mn^{2+} concentration in a Mn^{2+} buffer solution. In comparison with water alone, the TEA buffer had no effect on Mn^{2+} signal intensity. Mn^{2+} standards were measured on each day of data collection to adjust for day-to-day instrumental variations. Each titration point is the average of 2−3 separate measurements.

The data were fit [KaleidaGraph, Abelbeck] to eq 1 by assuming a simple model of j classes of independent, noninteracting sites (*35*). In this simple model, each type of site has a population of n_i identical sites, each of which has a dissociation constant of $K_{d(i)}$:

$$\frac{[Mn_b^{2+}]}{[hyb]} = \sum_{i=1}^{j} \frac{n_i[Mn_f^{2+}]}{(K_{d(i)} + [Mn_f^{2+}])} \quad (1)$$

Measurements of Hammerhead Ribozyme Activity. Activities and rate constants for the hammerhead ribozyme were determined with the 34-nt RNA enzyme and 5′-^{32}P-labeled 13-nt RNA substrate sequence of Figure 1a. ^{32}P labeling was performed with T4 polynucleotide kinase. Purified radiolabeled oligonucleotide samples were quantitated by UV absorbance as above. RNA−RNA hybrids consisting of a 1:1 ratio of enzyme to labeled substrate were annealed, at twice their final concentrations, as described above in TEA/pH, 7.8, and either 0.1 M NaCl or 1.0 M NaCl. Hybrids were then diluted to their final concentrations and ribozyme reactions were initiated by addition of various amounts of $MnCl_2$ and incubated for a given time at 21 °C. In 0.1 M NaCl the final hybrid concentration was 200 nM, whereas 5 μM hybrid (spiked with ^{32}P-labeled substrate) was used in 1 M NaCl in order to directly compare results with those obtained by EPR. Reactions were terminated by addition of 50 mM EDTA and 8 M urea and the substrate and product strands were separated by gel electrophoresis on 20% polyacrylamide gels. Labeled substrate and product strands were quantitated by phosphorimaging analysis.

Reaction rate constants (k) were determined by nonlinear least-squares analysis using the equation $P_t/P_f = (1 - e^{-kt})$, where P = [product/(product + substrate)] and P_t and P_f are product yields at time t and at completion of the reaction, respectively. Multiple rate determinations under the same conditions gave errors in k of ±∼10%. For this hammerhead, under the conditions used in the EPR titration experiment of pH 7.8 and 0.1 M NaCl, the relatively high maximum rates (k >10 min^{-1} at 2 mM Mn^{2+}) make accurate determinations of k by gel methods difficult at the higher Mn^{2+} concentrations. Kinetic measurements performed at pH 7.0 (in 5 mM MOPS and 100 mM NaCl), in which the maximum rate constant is $k \sim 5$ min^{-1} in 10 mM $MnCl_2$, show a parallel dependence on Mn^{2+} concentration (data not shown). The

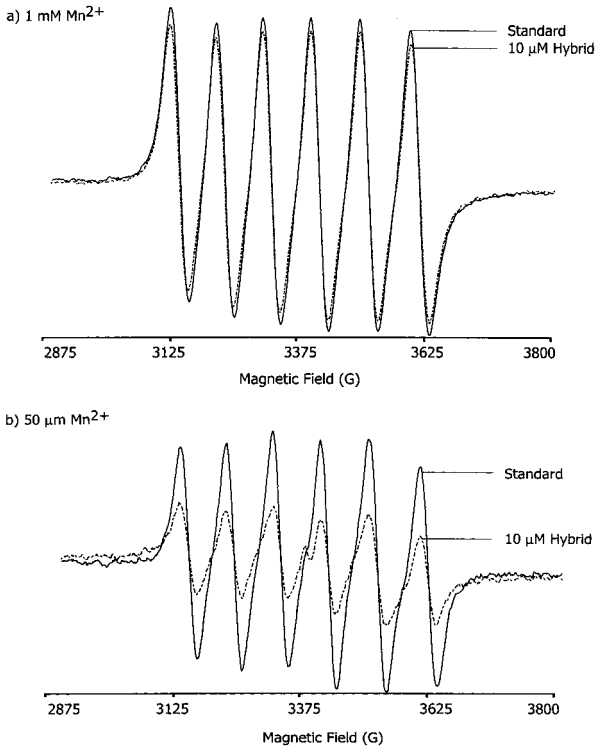

FIGURE 2: Mn^{2+} EPR spectra in the presence and absence of added hammerhead ribozyme. The diminution of the Mn^{2+} EPR spectra due to added RNA−DNA hybrid is shown for (a) 1 mM Mn^{2+} and (b) 50 μM Mn^{2+}. In each case the solid lines are standard samples of Mn^{2+} in buffer and dotted lines are samples having the same concentration of Mn^{2+} and 10 μM RNA−DNA hybrid hammerhead. Spectrometer conditions are given in Materials and Methods.

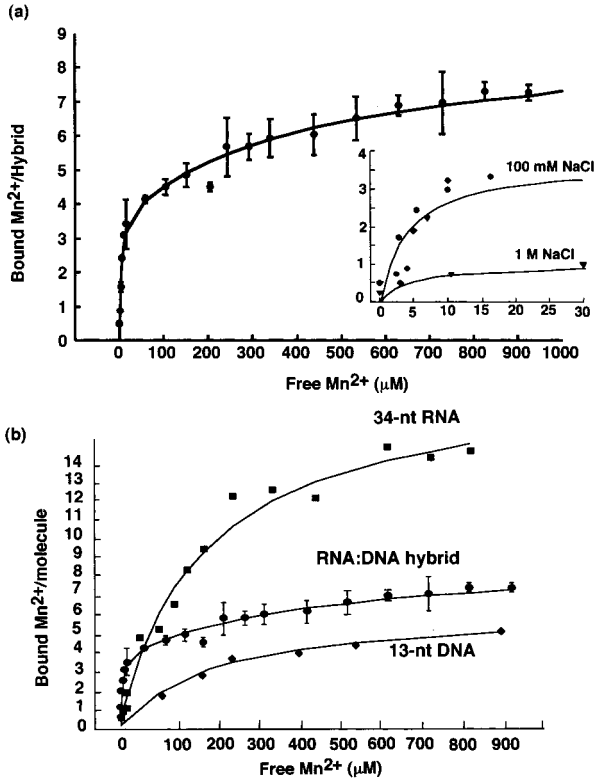

FIGURE 3: Mn^{2+} binding to hammerhead ribozyme. Metal-binding studies performed by monitoring loss of the room-temperature Mn^{2+} EPR signal as a measure of Mn^{2+} bound to the hammerhead hybrid. (a) Mn^{2+} binding isotherm for the RNA−DNA (main plot) and RNA−RNA (inset) hybrids of Figure 1a. (a, inset) Low Mn^{2+} concentration binding data for the RNA−DNA (●) and RNA−RNA (◆) hybrids at 100 mM NaCl and the RNA−DNA hybrid at 1 M NaCl (▼). (b) Mn^{2+} binding to the isolated 34-nt RNA enzyme (■) and 13-nt DNA substrate (◆) strands of Figure 1a. Samples are 5−10 μM (main plot) or 1 μM (a, inset) hybrid in 5 mM TEA, pH 7.8, and 100 mM NaCl and are fit (solid lines) as described in the text.

final product yield P_f was 75−85% of the initial substrate, and this number did not appear to depend on either NaCl or Mn^{2+} concentrations. These maximum extents of cleavage and the maximum observed rates of ≥ 1 min^{-1} are consistent with previous measures of the chemical step of the hammerhead reaction under single-turnover conditions (*36*). To best compare the spectroscopic studies with rate determinations, experiments were performed at 1:1 enzyme:substrate ratios and relatively high concentrations of hybrid, and the number of bound metal ions was calculated by assuming 100% hybrid formation. Consistent with this assumption, increasing the enzyme:substrate ratios to 2:1 and 3:1 did not change the measured rates of cleavage at 200 nM substrate and high levels of Mn^{2+}.

RESULTS

Mn^{2+} Binding Affinities for the RNA−DNA Hybrid Hammerhead. Addition of ribozyme to Mn^{2+} solutions causes a diminution of the Mn^{2+} EPR signal when compared to a standard in the absence of ribozyme. This diminution is due to a change in the electronic environment of the Mn^{2+} ion that is caused by interaction of the Mn^{2+} with the nucleic acid and can be quantitated to obtain the number of Mn^{2+} associated with the added ligand. The effect of 10 μM RNA enzyme/DNA substrate (RNA−DNA hybrid) hammerhead ribozyme on the EPR signal from 50 μM Mn^{2+} and 1 mM Mn^{2+} (Figure 2) demonstrates the sensitivity of the measurement. The change in EPR signal is easily detected in both samples, with the smaller difference (~10%) for the higher Mn^{2+}/hybrid samples being balanced by an increased signal: noise ratio under those conditions.

Figure 3a depicts a typical EPR-based Mn^{2+}-binding isotherm for the RNA−DNA hybrid hammerhead in 100 mM NaCl, pH 7.8. These data show a steep rise to ~4 bound Mn^{2+} as a function of free Mn^{2+}, followed by a more shallow increase to a total of ~8 Mn^{2+} bound per hybrid at 1 mM free Mn^{2+}. The binding curve was fit to a simple model of two different classes of binding sites per hammerhead, under the assumption that each class consists of multiple, identical, and noninteracting sites (*35*). Within this model, the curve of Figure 3a is best fit to ~4 Mn^{2+} sites having $K_{d1} \sim 4$ μM (tight type 1 sites), and ~5 sites with $K_{d2} \sim 460$ μM (weaker type 2 sites) (Table 1). Both the 34-nt RNA enzyme and 13-nt DNA substrate strand alone show only weaker Mn^{2+} affinities, with Mn^{2+} $K_d > 300$ μM (Figure 3b, Table 1). For these separate oligonucleotides, the total numbers of sites are roughly proportional to the length of the oligonucleotide, with dissociation constants comparable to those measured by other techniques (*37*). The higher affinity type 1 sites are found only in the presence of the RNA−DNA hammerhead hybrid.

The data of Figure 3a were obtained on an RNA−DNA hammerhead model that is chemically inactive due to the all-DNA substrate strand. To establish that the higher-affinity

Table 1: Summary of Mn^{2+} Affinities Measured by EPR

sample[a]	[NaCl] (mM)	n_1	$K_{d(1)}$ (μM)	n_2	$K_{d(2)}$ (μM)
RNA−DNA hammerhead[b]	100	3.7 ± 0.4	4 ± 1	5.2 ± 0.4	461 ± 130
	0	16.1 ± 1.6	39 ± 3	*c*	
	1000	1	≤10	*d*	
RNA−RNA (2′-OMe) hammerhead[e]	100	7.3 ± 0.4	32 ± 7	*c*	
34-nt RNA enzyme[b]	100			20 ± 2	320 ± 76
13-nt DNA substrate[b]	100			6.5 ± 0.8	366 ± 101

[a] Titrations performed with sample concentrations of 1−20 μM and in standard buffer conditions of 5 mM TEA, pH 7.8. [b] Hammerhead sequence shown in Figure 1a. [c] A model assuming two types of sites with different affinities did not significantly improve fit to present data. [d] Single-ion fit to data obtained at low Mn^{2+} concentrations (<80 μM free Mn^{2+}). [e] Hammerhead sequence shown in Figure 1b.

Mn^{2+} sites observed for the RNA−DNA hybrid are present for a hybrid with an all-RNA substrate, an RNA−RNA hybrid hammerhead also was investigated. As shown in the inset to Figure 3a, titration curves at low concentrations of added Mn^{2+} are very similar for the all-RNA and RNA−DNA hammerheads. EPR of the all-RNA hybrid could not be investigated at higher concentrations of Mn^{2+} due to cleavage activity (see below).

Addition of Mg^{2+} to the RNA−DNA hybrid in the presence of 1 mM Mn^{2+} releases all but one of the bound Mn^{2+} (data not shown), demonstrating that the majority of the Mn^{2+} sites in the hammerhead also can be occupied by Mg^{2+}.

Effect of Monovalent Cations on Mn^{2+} Binding to RNA−DNA Hybrid. Monovalent cations can have a strong effect on the interactions of divalent cations with nucleic acids (*38*, *39*) and this is observed for Mn^{2+} binding to the hammerhead ribozyme. Mn^{2+} binding studies were performed in 0 and 1.0 M NaCl, and the results are compared with those of Figure 3 that were obtained in the presence of 0.1 M NaCl.

In the absence of added Na^+, several additional Mn^{2+} sites are found for the RNA−DNA hammerhead hybrid (Figure 4a). Under these conditions the Mn^{2+} binding isotherms are best fit to a single set of ~16 Mn^{2+} sites with an average K_d ~ 40 μM. Addition of NaCl causes release of Mn^{2+} bound to the hybrid (Figure 4b). At a constant concentration of 1 mM Mn^{2+}, a steady decrease in the number of bound Mn^{2+} from ~15 to ~7 per hammerhead is observed with addition of 0−60 mM NaCl. As the NaCl concentration is increased beyond 60 mM, the apparent number of Mn^{2+} bound per hybrid remains constant at ~7 per hybrid (in 1 mM Mn^{2+}), up to 1 M NaCl.

By contrast with experiments performed at lower monovalent cation concentrations, Mn^{2+} binding to the hammerhead in 1 M NaCl gives rise to a sigmoidal binding isotherm, suggestive of cooperative binding behavior. In 1 M NaCl, a single Mn^{2+} binds at low concentrations of added Mn^{2+} (Figure 4a and Figure 3a, inset). This contrasts with the behavior in 100 mM NaCl, where a steep rise to 3−4 bound Mn^{2+} per hammerhead is observed at similar concentrations of added Mn^{2+}. In 1 M NaCl, however, at higher concentrations of added Mn^{2+} a transition occurs resulting in population of additional metal sites. By fitting data obtained at low Mn^{2+} concentrations (Figure 3a, inset), an apparent K_d of ≤ 10 μM is obtained for the tight Mn^{2+} site that is initially occupied in 1 M NaCl.

Comparison of the RNA−DNA Hybrid and an RNA−RNA-2′-O-methyl Hammerhead. For comparison between two different hammerhead models, Mn^{2+} binding curves for the RNA−RNA model of Figure 1b also were performed. This

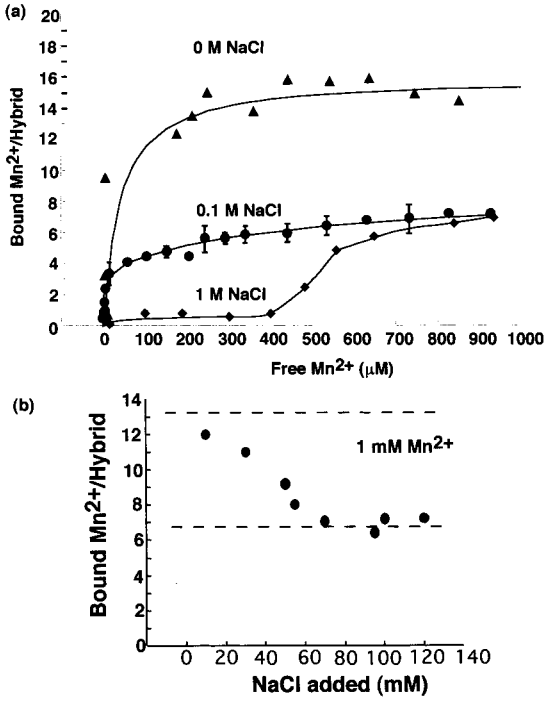

FIGURE 4: Influence of NaCl on Mn^{2+} binding to RNA−DNA hybrid hammerhead. (a) Mn^{2+}-binding data for the RNA−DNA hybrid hammerhead of Figure 1a in TEA, pH 7.8, and 0 M NaCl (▲), 100 mM NaCl (●), or 1 M NaCl (◆). The solid curves for 0 and 100 mM NaCl data are binding fits as described in the text and Table 1, and the solid line drawn through the 1 M NaCl data points is a smoothed curve that has no theoretical significance. (b) Influence of added NaCl on number of Mn^{2+} bound to the RNA−DNA hybrid in the presence of 1 mM Mn^{2+}. All samples are in TEA, pH 7.8, and 5−20 μM hammerhead hybrid.

sample, which is the same sequence as that used by Scott et al. for X-ray crystallography, has an inhibiting 2′-*O*-methyl substitution at the cleavage site (*11*). Mn^{2+} binding data obtained for this RNA−RNA(2′-OMe) hammerhead in 100 mM NaCl (Figure 5) were best fit to a single class of ~7 sites with average K_d ~ 30 μM. Although a more thorough data set will be required in order to distinguish the presence of the tighter sites in this other hammerhead, overall the RNA−RNA(2′-OMe) model appears to have very similar Mn^{2+}-binding characteristics to those of the RNA−DNA hammerhead model of Figure 1a.

Correlation of Populated Mn^{2+} Sites and Hammerhead Ribozyme Activity. Knowing the stoichiometry and affinities of the Mn^{2+} sites in the RNA−DNA model ribozyme, at any concentration of total Mn^{2+}, allows correlation of the cleavage activity of the RNA−RNA hammerhead with an estimated number of Mn^{2+} bound per ribozyme. Since the Mn^{2+} binding parameters of the RNA−DNA hybrid (Table

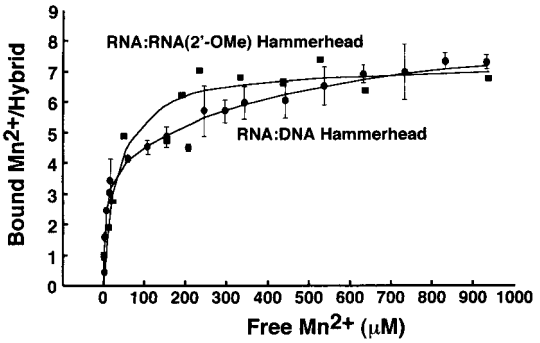

FIGURE 5: Comparison of Mn^{2+} binding affinities for two different hammerhead ribozymes. Mn^{2+} binding data for the RNA−DNA hybrid hammerhead of Figure 1a (●) and the RNA−RNA (2′-OMe) hammerhead of Figure 1b (■) in 100 mM NaCl in TEA, pH 7.8.

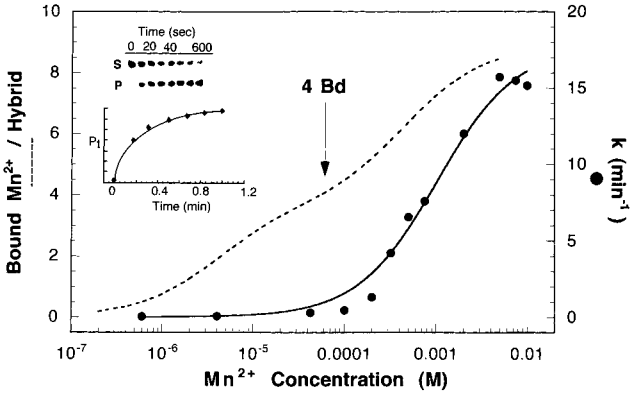

FIGURE 6: Comparison of ribozyme activity with number of bound Mn^{2+} in 100 mM NaCl. Ribozyme activity measurements performed for the RNA−RNA hammerhead of Figure 1a displayed as a function of added Mn^{2+} and (Mn^{2+} bound/RNA−DNA hammerhead). Rate constants (●, right axis) were measured following addition of metal ion to 200 nM RNA−RNA hybrid that was preincubated in TEA, pH 7.8, and 100 mM NaCl. Bound Mn^{2+}/hybrid (dotted line, left axis) was calculated for 200 nM hybrid by using the numbers and affinities determined for Mn^{2+} binding to the RNA−DNA hammerhead in 100 mM NaCl (Table 1, Figure 3). Inset: Example of a kinetic trace obtained at 200 nM hybrid and 320 μM Mn^{2+} (6 Mn/hybrid).

1) and the cleavage kinetics of the all-RNA hybrid were collected under the same solution conditions, at each total concentration of Mn^{2+} the rate constants for hammerhead cleavage can be directly compared to the estimated number of bound Mn^{2+} (Figure 6). The experiments shown in Figure 6 were performed at 0.1 M NaCl with the RNA−RNA hybrid having the same sequence as that in Figure 1a. A steep dependence of cleavage rate on added Mn^{2+} is observed, consistent with the previous studies that have shown that this rise depends on the type of metal ion and also on monovalent cations (*17*).

In 0.1 M NaCl, under Mn^{2+} concentrations at which the four high-affinity metal sites are populated, hammerhead activity remains minimal (Figure 6). The steep increase in activity appears to require population of the lower affinity sites, at Mn^{2+} concentrations corresponding to between 4 and 8 bound Mn^{2+} ([Mn^{2+}] $\geq \sim$200 μM). The midpoint of the rise in activity occurs at 1 mM Mn^{2+}. Above 5 mM Mn^{2+}, the observed activity does not increase, which is consistent with full population of the total of 8−9 Mn^{2+} sites indicated by the hammerhead binding isotherms.

The Mn^{2+} binding characteristics of the RNA−DNA hammerhead are markedly different in 1 M NaCl, and it is

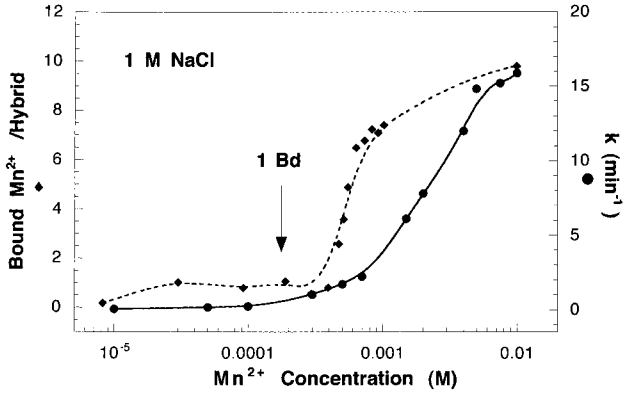

FIGURE 7: Comparison of ribozyme activity with number of bound Mn^{2+} in 1.0 M NaCl. Ribozyme activity measurements performed for the RNA−RNA hammerhead of Figure 1b displayed as a function of added Mn^{2+} and Mn^{2+} bound per hammerhead. Rate constants (●, right axis) were measured following addition of metal ion to 5 μM hybrid that was preincubated in TEA, pH 7.8, and 1.0 M NaCl. Bound Mn^{2+}/hybrid (◆, left axis) are the data obtained for 5 μM RNA−DNA hybrid hammerhead in 1 M NaCl that are displayed in Figure 3, here replotted against total Mn^{2+}. The dotted line drawn through the bound Mn^{2+} data points is a smoothed curve that has no theoretical significance.

therefore of interest to examine the relationship between Mn^{2+} and RNA−RNA hammerhead activity under these conditions. These activity results are displayed in Figure 7. In 1 M NaCl, as in 100 mM NaCl, the measured cleavage rate constants rise steeply as a function of added Mn^{2+}. The single high-affinity Mn^{2+} site is populated at low concentrations of Mn^{2+}. As is the case in 100 mM NaCl, however, appreciable cleavage activity does not occur until Mn^{2+} concentrations are reached corresponding to population of the additional metal sites on the ribozyme. A slight increase in activity occurs in Mn^{2+} concentrations at the beginning of the cooperative transition of the binding curve ([Mn^{2+}] $\sim$ 500 μM), and maximum activity occurs at $\sim$10 mM Mn^{2+}, where 9−10 bound Mn^{2+} are measured by EPR. A slightly higher Mn^{2+} concentration of $\sim$2 mM Mn^{2+} is found for the midpoint of activity in 1 M NaCl.

DISCUSSION

An important step in understanding metal-dependent RNA catalysis is the determination of the numbers and affinities of metal binding sites under defined solution conditions. A direct measure of divalent metal ion binding to biomolecules in dilute solution can be obtained by monitoring the room-temperature EPR signal from Mn^{2+}, which substitutes for Mg^{2+} and supports 100% hammerhead cleavage activity that is observed with Mg^{2+} (*17*, *18*). For the two hammerhead sequences that have been characterized by X-ray crystallography (Figure 1), several Mn^{2+} sites with relatively high affinities are observed by the EPR-based titration method (Table 1). Not unexpectedly, despite the different reports of divalent ion populations in their respective crystal structures, both of these hammerheads exhibit similar Mn^{2+}-binding behavior under solution conditions.

In 100 mM NaCl, approximately 4 high-affinity sites characterized by $K_d \sim 4$ μM and $\sim$5 lower-affinity sites with $K_d \sim 460$ μM are found for the RNA−DNA hybrid of Figure 1a. The high-affinity sites are not present in either the RNA

or DNA alone and apparently are created upon formation of the hammerhead hybrid in solution. These hammerhead metal-binding characteristics are similar to those found for transfer RNAs (reviewed in ref *39*). In the presence of monovalent cations, high-affinity divalent cation sites (n = 1−6) in tRNA are reported with K_ds in the micromolar range and are assumed to be correlated with specific divalent cation-binding sites found populated in tRNA X-ray crystal structures (*39*−*41*). Additional classes of Mn^{2+} ($K_d \sim 200$ μM, 0.1 M TEA) (*39*) and Mg^{2+} ($K_d \sim 1-5$ mM, 80−170 mM NaCl) (*39*, *42*) interactions also have been found for tRNA. Intermediate and lower-affinity interactions with divalent cations also have been characterized in other structured RNAs (*43*−*46*).

Structured RNA molecules may be expected to exhibit a range of different types of metal interactions. The association of counterions with nucleic acids has been described in terms of polyelectrolyte theories, which have been developed mainly for unstructured (linear) chains and predict association of positively charged ions that are characterized as atmospheric or condensed on the polyanion (*47*, *48*). Both monovalent and divalent cations can satisfy this type of nonspecific binding, and the affinities of divalent cations decrease significantly with increasing monovalent cation concentration (*38*). In the case of the hammerhead model, the loss of approximately half of the bound Mn^{2+} (∼8 sites) measured in 1 mM Mn^{2+} between 0 and 60 mM NaCl (Figure 4b) is likely due to nonspecific charge screening interactions that can be satisfied with either monovalent or divalent cations.

The remaining bound Mn^{2+} ions are observed in both 0.1 and 1 M NaCl and therefore appear to occupy more specific sites in the hammerhead ribozyme. Cations may be localized at sites that are created in RNA structures by closely spaced negative charges or electronegative groups. Binding to these negatively charged pockets may be mainly electrostatic and depend on the size and charge of the ion (*44*−*46*). Ions also may be stabilized by hydrogen bonding through outer-sphere interactions. More specific coordination sites exist in RNA structures in which the metal ion makes inner-sphere contact with two or more ligands such as the nitrogen bases or the phosphodiester oxygens. Although several RNA−metal interactions exhibiting a mixture of binding environments have been predicted by X-ray crystallography (*10*−*14*, *40*, *41*, *49*, *50*), there are few examples of affinity constants that can be used to guide studies in solution. The high-affinity tRNA sites are examples of site-bound ions. Site-specific cation affinities of $K_a \sim (1-10) \times 10^3$ M^{-1} [in 0.1 M KCl (*45*) and 1.6 M NH_4Cl (*46*)], similar to the type 2 sites observed for the hammerhead, have been proposed from thermodynamic measurements of structured RNA molecules. Further characterization of ion specificity will aid in elucidating the properties of the hammerhead cation binding sites.

In the present studies, the Mn^{2+} EPR signal is used to measure ions interacting with nucleic acid samples. In this technique, the assumption is made that all bound ions have undetectable EPR signals at room temperature. The loss of the EPR signal is due to extreme line broadening caused by an increase in the zero-field splitting parameter D, which affects the Mn^{2+} electron spin relaxation rate as $T_2 \sim |D|^2$. Replacement of a water ligand in $Mn(H_2O)_6^{2+}$ by another ligand is thought to increase D sufficiently to broaden the room-temperature Mn^{2+} signal beyond detection (*51*). Immobilization on the EPR time scale of hydrated Mn^{2+} ions may also result in loss of the room-temperature EPR signal. Lesser perturbations, however, such as fluctuations in the environment of the outer-sphere ligands that are faster than the EPR time scale, would lead instead to a smaller amplitude change with detectable broadening of the Mn^{2+} EPR signal (*51*). In the case of the hammerhead ribozyme, no significant change in line width is detected in the Mn^{2+} EPR signal in the presence and absence of added nucleic acid, indicating that loss of signal is due to Mn^{2+} ions that are localized in binding sites on the nucleic acid. It should be noted, however, that very weakly bound ions ($K_d \geq \sim 1$ mM) may not be detected by these experiments, because of both the concentration range of the data and the difficulty in detecting a very small population of perturbed (i.e., broadened) EPR signal. It must also be noted, with respect to using Mn^{2+} as a probe of cation sites, that nucleic acid−Mn^{2+} affinities are generally higher than those for Mg^{2+} and Mn^{2+} tends to exhibit more inner-sphere interactions than found for Mg^{2+}. Thus, although Mn^{2+} replaces Mg^{2+} in activating the ribozyme, the specific metal−RNA interactions may differ between the two ions.

Under conditions of 0.1 M NaCl and at pH 7.8, the hammerhead does not show cleavage activity until Mn^{2+} concentrations are above those required to populate the four high-affinity sites. Cleavage rates then begin to rise as Mn^{2+} concentrations reach those necessary to populate the 4−5 intermediate-affinity type 2 sites, and rates are at a maximum under conditions where a total of ∼9 Mn^{2+} ions are bound. In 1 M NaCl, cleavage rates are minimal at Mn^{2+} concentrations where the single high-affinity site is populated and do not rise until Mn^{2+} concentrations are reached corresponding to the apparent cooperative transition that results in population of the ∼9−10 Mn^{2+} sites under these conditions. In both 1 and 0.1 M NaCl, half-maximal activity is reached at 1−2 mM Mn^{2+}, corresponding to a lower-affinity interaction than those measured in these Mn^{2+} binding studies. The EPR experiments performed here monitor metal binding only to the ground-state of the ribozyme, and the results cannot preclude binding of one or more additional metal ions during the course of the ribozyme reaction. These data indicate, however, that in its most active state the hammerhead is populated by several Mn^{2+} ions with a mixture of affinities. The identities of these sites, and their relationship to hammerhead activity, are under current investigation.

Reasonable candidates for high-affinity metal sites in the hammerhead include those previously identified at G10.1/A9 by site-specific phosphorothioate substitution (*23*) and at G5 by Tb^{3+} competition studies (*14*). The G10.1/A9 site in particular has predicted inner-sphere coordination from the phosphodiester of A9 and the N7 of G10.1 that might correspond to a relatively high-affinity metal interaction in solution conditions. Relevant to the current study, Mg^{2+}-dependent structural transitions in hammerhead ribozymes have been characterized by native gel electrophoresis (*24*) and fluorescence resonance energy transfer experiments (*25*) with apparent Mg^{2+} affinities corresponding to $K_{a1}(Mg^{2+})$ $\sim 10^4$ M^{-1} and $K_{a2}(Mg^{2+}) \sim 1$ mM^{-1}. The higher-affinity Mg^{2+}-induced transition is affected by mutations at position A14, whereas mutations at the G5 site cause loss of the structural transition associated with the lower apparent Mg^{2+}

affinity. It will be of interest to determine if similar mutations affect the Mn^{2+} sites characterized in the present study.

ACKNOWLEDGMENT

We are grateful to Professor David Giedroc for helpful discussions and to Carla Theimer and Paul Nixon for expert assistance in RNA preparation.

REFERENCES

1. Cech, T. R. (1993) in *The RNA World* (Gesteland, R., and Atkins, J. F., Eds.) pp 239−270, Cold Spring Harbor Laboratory Press, Cold Spring Harbor, NY.
2. Birikh, K. R., Heaton, P. A., and Eckstein, F. (1997) *Eur. J. Biochem. 245*, 1−16.
3. Pan, T., Long, D. M., and Uhlenbeck, O. C. (1993) in *The RNA World* (Gesteland, R., and Atkins, J. F., Eds.) pp 271−302, Cold Spring Harbor Laboratory Press; Cold Spring Harbor, NY.
4. Yarus, M. (1993) *FASEB J. 7*, 31−39.
5. Pyle, A. M. (1993) *Science 261*, 709−714.
6. Bratty, J., Chartrand, P., Ferbeyre, G., and Cedergren, R. (1993) *Biochim. Biophys. Acta 1216*, 345−359.
7. McKay, D. B. (1996) *RNA 2*, 395−403.
8. Wedekind, J. E., and McKay, D. B. (1998) *Annu. Rev. Biophys. Biomol. Struct. 27*, 475−502.
9. Narlikar, G. J., and Herschlag, D. (1997) *Annu. Rev. Biochem. 66*, 19−59.
10. Pley, H. W., Flaherty, K. M., and McKay, D. B. (1994) *Nature 372*, 68−74.
11. Scott, W. G., Finch, J. T., and Klug, A. (1995) *Cell 81*, 991−1002.
12. Scott, W. G., Murray, J. B., Arnold, J. R. P., Stoddard, B. L., and Klug, A. (1996) *Science 274*, 2065−2069.
13. Murray, J. B., Terwey, D. P., Maloney, L., Karpeisky, A., Usman, N., Beigelman, L., and Scott, W. G. (1998) *Cell 92*, 665−673.
14. Feig, A. L., Scott, W. G., and Uhlenbeck, O. C. (1998) *Science 279*, 81−84.
15. Simorre, J.-P., Legault, P., Hangar, A. B., Michiels, P., and Pardi, A. (1997) *Biochemistry 36*, 518−525.
16. Hermann, T., Auffinger, P., Scott, W. G., and Westhof, E. (1997) *Nucleic Acids Res. 25*, 3421−3427.
17. Dahm, S. C., and Uhlenbeck, O. C. (1991) *Biochemistry 30*, 9464−9469.
18. Dahm, S. C., Derrick, W. B., and Uhlenbeck, O. C. (1993) *Biochemistry 32*, 13040−13045.
19. Steitz, T. A., and Steitz, J. A. (1993) *Proc. Natl. Acad. Sci. U.S.A. 90*, 6498−6502.
20. Lott, W. B., Pontius, B. W., and von Hippel, P. H. (1998) *Proc. Natl. Acad. Sci. U.S.A. 95*, 542−547.
21. Slim, G., and Gait, M. J. (1991) *Nucleic Acids Res. 19*, 1183−1188.
22. Zhou, D.-M., and Taira, K. (1998) *Chem. Rev. 98*, 991−1026.
23. Peracchi, A., Beigelman, L., Scott, E. C., Uhlenbeck, O. C., and Herschlag, D. (1997) *J. Biol. Chem. 272*, 26822−26826.
24. Bassi, G. S., Murchie, A. I. H., and Lilley, D. M. J. (1996) *RNA 2*, 756−768.
25. Bassi, G. S., Murchie, A. I. H., Walter, F., Clegg, R. M., and Lilley, D. M. J. (1997) *Eur. J. Mol. Biol. 16*, 7481−7489.
26. Menger, M., Tuschl, T., Eckstein, F., and Porschke, D. (1996) *Biochemistry 35*, 14710−14716.
27. Cohn, M., and Townsend, J. (1954) *Nature 173*, 1090−1091.
28. Woody, A.-Y. M., Eaton, S. S., Osumi-Davis, P. A., and Woody, R. W. (1996) *Biochemistry 35*, 144−152.
29. Reed, G. H., and Markham, G. D. (1984) *Biol. Magn. Reson. 6*, 73−142.
30. Danchin, A., and Guéron, M. (1970) *Eur. J. Biochem. 16*, 532−536.
31. Wang, K. Y., Gerena, L., Swaminathan, S., and Bolton, P. H. (1995) *Nucleic Acids Res. 23*, 844−848.
32. Milligan, J. F., and Uhlenbeck, O. C. (1989) *Methods Enzymol. 180*, 51−62.
33. Warshaw, M. M., and Tinoco, I. (1966) *J. Mol. Biol. 20*, 29−38.
34. Eaton, S. S., and Eaton, G. R. (1977) *Anal. Chem. 49*, 1277−1278.
35. Klotz, I. M. (1997) *Ligand−Receptor Energetics*, John Wiley, New York.
36. Fedor, M. J., and Uhlenbeck, O. C. (1992) *Biochemistry 31*, 12042−12054.
37. Schreier, A. A., and Schimmel, P. R. (1974) *J. Mol. Biol. 86*, 601−620.
38. Record, M. T., Lohman, T. M., and de Haseth, P. (1976) *J. Mol. Biol. 107*, 145−158.
39. Schimmel, P. R., and Redfield, A. G. (1980) *Annu. Rev. Biophys. Bioeng. 9*, 181−221.
40. Jack, A., Ladner, J. E., Rhodes, D., Brown, R. S., and Klug, A. (1977) *J. Mol. Biol. 111*, 315−328.
41. Holbrook, S. R., Sussman, J. L., Warrant, R. W., Church, G. M., and Kim, S. H. (1977) *Nucleic Acids Res. 4*, 2811−2820.
42. Reid, S. S. and Cowan, J. A. (1990) *Biochemistry 29*, 6025−6032.
43. Beebe, J. A., Kurz, J. C., and Fierke, C. A. (1996) *Biochemistry 35*, 10493−10505.
44. Gluick, T. C., Wills, N. M., Gesteland, R. F., and Draper, D. E. (1997) *Biochemistry 3*6, 16173−16186.
45. Laing, L. G., Gluick, T. C., and Draper, D. E. (1994) *J. Mol. Biol. 237*, 577−587.
46. Bukhman, Y. V., and Draper, D. E. (1997) *J. Mol. Biol. 273*, 1020−1031.
47. Manning, G. S. (1979) *Acc. Chem. Res. 12*, 443−449.
48. Anderson, C. F., and Record, M. T., Jr. (1995) *Annu. Rev. Phys. Chem. 46*, 657−700.
49. Holbrook, S. R., and Kim, S.-H. (1997) *Biopolymers 44*, 3-21.
50. Correll, C. C., Freeborn, B., Moore, P. B., and Steitz, T. A. (1997) *Cell 91*, 705−712.
51. Ottaviani, M. F., Montalti, F., Romanelli, M., Turro, N. J., and Tomalia, D. A. (1996) *J. Phys. Chem. 100*, 11033−11042.

BI981425P